Periodic orbit–Quantum mechanical investigation of the inversion mechanism of Ar_3

Raul Guantes, Anastasios Nezis,[a] and Stavros C. Farantos[b]
Institute of Electronic Structure and Laser, Foundation for Research and Technology-Hellas, Iraklion, Crete, 711 10, Greece

(Received 20 May 1999; accepted 20 September 1999)

The inversion mechanism of a T-shaped Ar_3 is studied both classically and quantum mechanically. Regular states, localized in the region of the transition state for the inversion of the axial argon atom are found and are assigned by the symmetric stretch stable periodic orbits which emanate from the saddle point of the potential. These states inhibit the inversion process. States which promote the inversion are mainly irregular, but a few of them are localized and they have their nodes perpendicularly arranged along periodic orbits which originate from saddle node bifurcations. The two types of periodic orbits, inhibiting and isomerizing, are used to produce distinctly different spectra and to extract the corresponding eigenfunctions by solving the time dependent Schrödinger equation using a variable order finite difference method [J. Chem. Phys. **111**, 10827 (1999), preceding paper]. © *1999 American Institute of Physics.* [S0021-9606(99)30247-6]

I. INTRODUCTION

One elementary chemical reaction is the inversion of a molecule. Generally, inversion may be seen as an isomerization reaction between two equivalent minimum energy conformations which correspond to two symmetric minima on the potential energy surface (PES). Isomerization occurs by exciting the molecule to a vibrational state which has appreciable probability amplitude in both minima. At energies where the molecule isomerizes the motions of atoms are expected to be irregular because of the nonlinearity and coupling of the potential function[1] close to and above the barrier of isomerization.

The progress of high resolution spectroscopy at excited vibrational states in the last years reveals that, contrary to our expectations, spectra at high energies can be analyzed with simple spectroscopic models in reduced dimension space.[2] These models are described by resonance Hamiltonians which have regular localized eigenfunctions, and this explains the regular patterns frequently found in vibrationally excited spectra.

Semiclassical approximations seem to provide a satisfactory theory for the localization of the wave functions. Particularly, it has been found that periodic orbits may be used as diagnostic tools for the localization in quantum mechanics.[1] Regular wave functions have recognizable nodal structures which follow the patterns of periodic orbits.[3] For high vibrational excitations of particular interest are those periodic orbits which emerge from saddle node (SN) bifurcations. These periodic orbits appear suddenly in phase space as pairs of one stable and one unstable family. This is important, since the emergence of a SN bifurcation signals the existence of stable domains in phase space embedded in a usually chaotic region. The correspondence of stable periodic orbits to quantum eigenfunctions[4] dictates quantum mechanical localization as well.

In double well potentials, periodic orbits which connect the two minima are mainly associated with SN bifurcations. We have shown this for bound[5,6] and unbound[7] molecular systems. A recent example with a spectroscopic signature for the SN states is the HCP molecule. *Dispersed fluorescence* and *stimulated emission pumping* vibrational-rotational spectroscopy[8,9] of the bending mode has shown that the rotational constants are different for the normal mode type bending states (states associated with the minimum of the potential) and the isomerizing bending states. Although *ab initio* calculations for the ground electronic state of HCP predict a saddle point for the CPH conformation and not a minimum, it has been demonstrated that the vibrational states which lead loosely speaking to isomerization of the hydrogen atom from the carbon to phosphorus side are associated with SN periodic orbits.[10–12]

Homonuclear triatomic molecules, A_3, can also show inversion of the axial atom with respect to the A−A bond. In this case, the transition state is a collinear configuration with the axial A atom sitting in the middle of the A−A bond. An example is H_3^+, for which it has been shown that localized isomerizing states exist and are marked by similar types of periodic orbit named ''horseshoe.''[13]

The van der Waals system Ar_3 is another example which can show inversion of the axial Ar atom. The weak forces among the atoms dictate that the molecule executes floppy irregular motions. Early studies on this system revealed that the trajectories even close to the minimum have positive Lyapunov exponents.[14,15] However, more recent classical mechanical studies[16,17] have shown a nonstatistical inversion dynamics in spite of the fact that the phase space is dominated by chaotic trajectories above the inversion threshold.

[a]Also at Department of Physics, University of Crete, Iraklion 711 10, Crete, Greece.
[b]Also at Department of Chemistry, University of Crete, Iraklion 711 10, Crete, Greece

Vibrational quantum mechanical calculations for the rotationless system have recently been presented by Wright and Hutson.[18] What is surprising in these calculations is the regularity and localization of a few eigenfunctions above the barrier of inversion found among irregular eigenstates with no recognizable nodal patterns.

In this article we want to investigate more thoroughly the inversion dynamics and spectroscopy of the van der Waals system, Ar_3. Thus, we apply the periodic orbit method (POM) introduced before.[1] Families of periodic orbits which originate from the saddle point of the potential function as well as saddle node bifurcations are located to explore the structure of phase space in regions where inversion takes place. These periodic orbits are then used to guide wave packets which are propagated by solving the time dependent Schrödinger equation. The important role of the initial phase of the wave functions (assigned by the momenta of POs) results in completely different spectra produced at high energies, where wave packets with the same amplitudes but different phases serve to excite the molecule in different modes.

We apply a new algorithm and recent ideas on high order finite difference method[19] to obtain the solutions of the Schrödinger equation which are then compared with the results of fast Fourier pseudospectral calculations. The curved shape of the potential function leads the finite difference method to a superior position since it allows us to choose the grid points in an energetically optimum way and to apply the appropriate boundary conditions. Details of the finite difference methods are presented in the companion paper.[20]

II. NUMERICAL DETAILS

Both classical and quantum calculations are performed for C_{2v} geometries of the three argon atoms using the Hamiltonian:

$$H=\frac{p_1^2}{2\mu_1}+\frac{p_2^2}{2\mu_2}+V(x_1,x_2). \tag{1}$$

x_1 is the position of the axial argon atom along a perpendicular axis to the middle of the bond length, x_2, of the other two argon atoms. μ_1 is the reduced mass of the axial argon atom with respect to Ar_2 and μ_2 the reduced mass of Ar_2. The potential function, $V(x_1,x_2)$, is determined from the sum of the three Ar–Ar interactions. The latter are described by the empirical potential of Aziz and Slaman.[21]

The same potential has been used by Dumont and Jain[16] in a classical statistical study of the inversion dynamics. It supports two symmetric minima accessible through the inversion process. The minima are at $(x_1,x_2)=(\pm 6.15,7.099)a_0$ the energy of which is taken to be equal to zero. The saddle point between these two minima has the collinear geometry of $(x_1,x_2)=(0.0,14.19)a_0$, and energy 140.38 K above the minimum. The energies are measured in Kelvin.[16] The dissociation limit to $Ar+Ar_2$ is 286.415 K. In Fig. 1 we show contour plots of the potential function covering the energy range between 50 and 300 K. In the insert the coordinates x_1 and x_2 are defined.

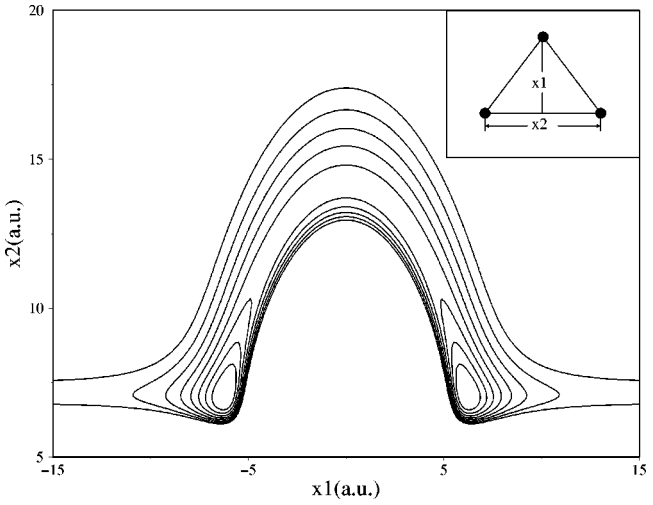

FIG. 1. Potential energy contours for the Ar_3 molecule between 50 and 300 K (1 K=0.695 cm^{-1}). In the inset the molecule with the coordinate system is shown.

Methods for locating periodic orbits have been described before.[22] Usually, a quasi-Newton method is employed to find the proper initial conditions for closing the trajectory. However, we are interested in locating families of periodic orbits for a range of energies. Thus, continuation methods are equally important.[23] Through continuation of the principal families, i.e., families which emerge from the stationary points of the potential, we find bifurcations, and gradually we unravel the structure of phase space for a domain of total energies. The stability properties of each periodic orbit, i.e., the behavior of the surrounding trajectories with time, are then examined by calculating the eigenvalues of the monodromy matrix.[24,25]

Spectra and quantum mechanical wave functions are calculated by solving the time dependent Schröndiger equation using the Fourier pseudospectral (PS) method[26] and a fast and numerically robust variable order finite difference (FD) method. Using recurrence relations for the Lagrange interpolation polynomials a general algorithm for computing any derivative of a function at arbitrary points and at any order of approximation have been presented by Fornberg.[19,27] This allows us to check systematically the convergence of the spectra by increasing the order of approximation of the second derivatives. It can be shown that FD methods at the infinity order of approximation are equivalent to spectral methods. However, the desired accuracy is achieved for finite orders and this makes FD methods competitive to pseudospectral techniques. As the number of degrees of freedom increases the flexibility of choosing the grid points according to physical criteria makes FD methods superior to pseudospectral techniques.[20] This is demonstrated even for the present 2D system for which rectangular grids, usually employed in fast Fourier transform methods, will lead to an inefficient configuration space sampling.

Some ways to optimize grids with FFT algorithms have been proposed[28] but they are less general and not as easy to handle as a FD procedure. Finite differences not only offer flexibility in grid sampling, a property which is shared with

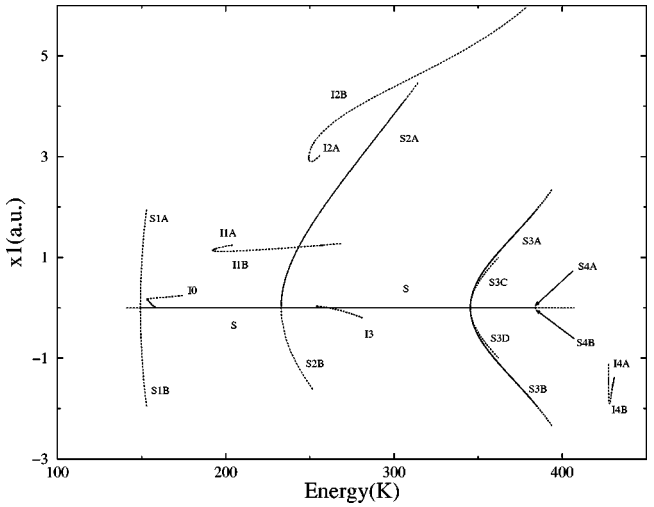

FIG. 2. Continuation/bifurcation diagram for the principal family emanating from the saddle point of the potential (*S* family) and some saddle node POs (*I* families). Solid lines denote stable POs and dashed lines unstable ones.

the discrete variable representation (DVR) Pseudospectral methods, but also result in having a smaller number of nonzero Hamiltonian matrix elements than DVR.[29,30] This is also in the spirit of other local and semilocal methods such as the distributed approximated functionals (DAF).[31] Numerical details of the implementation of FD method in Ar_3 are given in the next section.

III. RESULTS AND DISCUSSION

A way to represent families of periodic orbits as the total energy or other control variables change are via continuation/bifurcations (C/B) diagrams. These are plots of the initial conditions of the periodic orbits or their periods as functions of the total energy. Generally, C/B diagrams reveal the stable and unstable regions of phase space, and thus, they provide global information about the dynamics of the molecule. Their importance in molecular systems stems in the expected correspondence among stable and short period periodic orbits and quantum mechanical eigenfunctions.

Continuation/bifurcation diagrams are constructed for each stationary point of the potential function. The existence of the principal families of POs which originate from the stationary points are guaranteed by Weinstein[32] and Moser[33] theorems. Since here we are interested in the inversion dynamics of Ar_3, we discuss the C/B diagram of the saddle point of the potential.

There is one principal family which emerges from the saddle point. In Fig. 2 we plot a projection of the continuation/bifurcation diagram, the initial x_1 coordinate of each located periodic orbit versus the total energy. Continuous lines denote stable POs and dashed lines unstable POs. The periodic orbits of the principal family correspond to the symmetric stretch of the three atoms in collinear configuration. The principal family is denoted by *S* in Fig. 2 and is initially unstable in the direction of x_1 axis. Interestingly enough, this family turns to stable POs about 10 K above the saddle point. At the critical energy where the *S* turns from

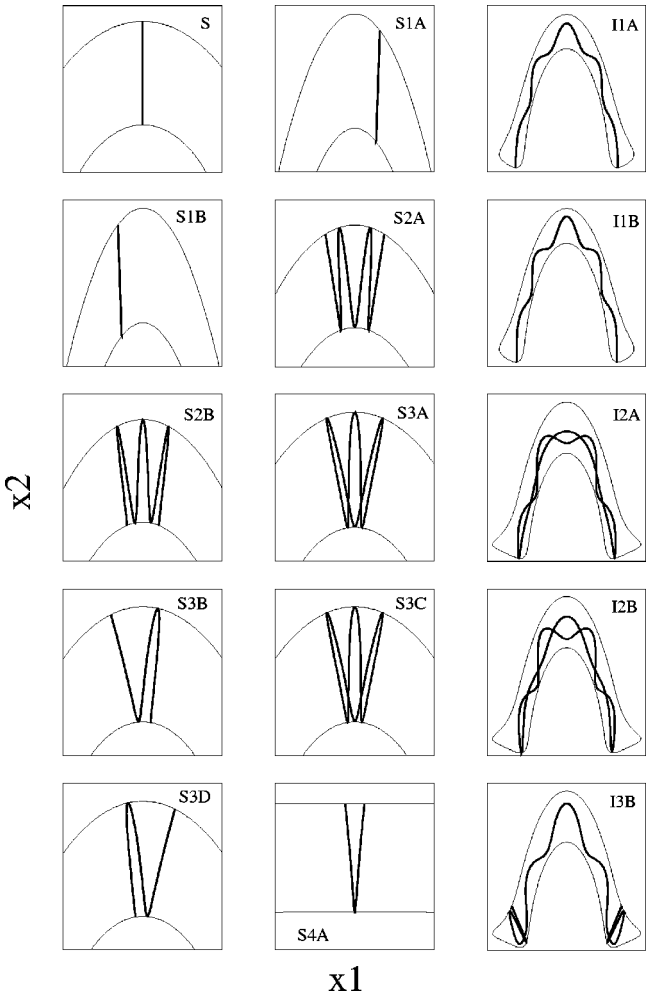

FIG. 3. Representative periodic orbits projected on the configuration plane. The potential contours at the same energy with the PO are also shown.

unstable to stable two new unstable families the $(S1A,S1B)$ are born.[24,25,34] The stability island which is formed around the stable periodic orbits makes the isomerizing chaotic trajectories to be trapped around this region of phase space for a long time, something which is manifested in the inversion dynamics with the deviations from the statistical behavior.[15,16]

In the diagram of Fig. 2 we can see the bifurcation of other families as well as the change of *S* back to unstable POs at energy 390 K. Plots of representative POs are shown in Fig. 3 and initial conditions for one periodic orbit of each family are stored in Table I. It is interesting to note the simultaneous bifurcation of four new families, $S3$. The $S3A$ and $S3C$ POs have the same projection on the (x_1,x_2) plane but they have a reflection symmetry $(p_{1,2}\rightarrow -p_{1,2})$ when they are projected on a coordinate-momentum plane.

The other class of POs with physical interest is this which emerges from saddle node bifurcations and a few of them are shown in Fig. 2. We use the symbols $I0$, $I1$, $I2$, etc. to denote their association with the inversion. Indeed, the saddle node POs are those which connect the two minima and the symmetric ones can easily be found. They appear always with two branches, one stable and one unstable. The stable one may turn to unstable shortly after its generation

TABLE I. Energies E in Kelvin, periods T in time units, and distances in Bohrs for selected periodic orbits. λ is the real part of the eigenvalue of the monodromy matrix. 1 time unit = 7.638 185 ps.

	E	x_1	x_2	p_1	p_2	T	λ
S	355.193 020	0.0	14.186 500	0.0	7.041 294	0.436 900	−0.618 740
S1A	150.009 681	0.884 718	14.186 500	0.351 702	1.417 406	0.398 700	1.271 292
S1B	150.009 681	−0.884 718	14.186 500	−0.351 702	1.417 406	0.398 700	1.271 292
S2A	240.391 374	1.007 793	14.186 500	1.566 077	4.586 023	1.493 700	0.987 384
S2B	240.559 217	−1.006 265	14.186 500	−1.187 946	4.674 673	1.494 700	1.175 233
S3A	355.056 362	0.811 452	14.186 500	2.029 015	6.810 171	1.289 199	0.977 896
S3B	355.054 526	−0.727 657	14.186 500	−2.353 375	6.733 869	1.290 099	1.228 331
S3C	355.056 362	−0.811 452	14.186 500	−2.029 015	6.810 171	1.289 199	0.977 896
S3D	355.054 526	0.727 657	14.186 500	2.353 375	6.733 869	1.290 099	1.228 331
S4A	384.132 047	0.012 382	14.186 500	0.063 627	7.500 394	1.187 799	0.999 201
I0	154.214 888	0.136 201	14.245 908	2.0463 811	−0.070 579	3.896 184	1.0E+06
I1A	192.557 996	−1.147 537	14.186 500	2.731 487	2.466 677	1.548 220	−0.985 970
I1B	194.143 570	1.118 703	14.186 500	−2.565 726	2.672 989	1.604 629	58.861 806
I2A	255.184 832	2.997 235	14.186 500	−4.411 452	0.874 535	1.163 199	−9.614 324
I2B	255.087 869	−1.699 774	14.186 500	−5.507 814	1.431 645	1.235 299	40.957 072
I3	264.262 548	−0.022 283 7	15.795 319	−3.934 940	−0.053 452 8	2.405 55	0.13E+06
I4A	430.002 365	7.186 733	14.186 500	−2.044 194	3.040 661	1.208 299	−0.818 486
I4B	427.603 359	10.648 308	14.186 500	0.654 135	1.546 986	4.057 799	3.924 245

and that depends on the particular system. The real value of the eigenvalue λ of the monodromy matrix given in Table I reveals that the I type POs are mainly unstable.

To estimate the extension of the stable region around stable periodic orbits in Fig. 4 we plot Poincaré surfaces of sections, one with the $x_2 = 14.1865 a_0$ and one with $x_1 = 0 a_0$ and at energy of 192.4 K. It is interesting to note that the S periodic orbits have a quite extended stable region around them [Fig. 4(a)]. Contrary to that, the stable region around the $I1A$ PO is very small. Inspection of other Poincaré surfaces of sections for several energies reveals a mostly chaotic phase space for energies above the saddle point but with islands of stability embedded in it.

What is the behavior of quantum mechanics in a mixed chaotic/regular classical phase space as described above? To investigate the quantum dynamics we solve the time dependent Schrödinger equation. The time propagator is expanded in a series of Chebyshev polynomials.[26] The action of the Laplacian on the wave function is determined both by FFT and a variable order FD method.[20]

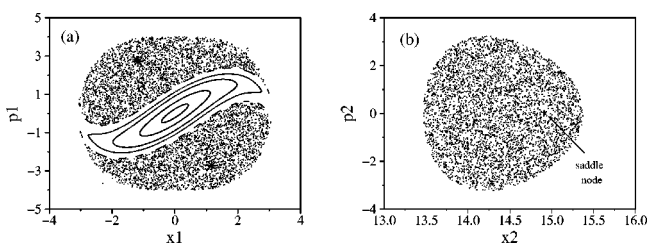

FIG. 4. Poincaré surfaces of section at $E = 192.4$ K, and $x_2 = 14.1865\ a_0$ (a) and $x_1 = 0$ (b). The small stability islands which correspond to the saddle node PO of the family $I1A$ (see Fig. 2) have been marked with stars in (a). The big island corresponds to the saddle family S. Note that this stable PO is the border of the energy shell in panel (b).

Two Gaussian wave packets are launched

$$\phi(x_1,x_2) = \prod_{k=1}^{2} (2\pi\alpha_k^2)^{-1/4} \exp[-(x_k - x_{k0})^2/4\alpha_k^2 + i p_{k0}(x_k - x_{k0})/\hbar], \quad (2)$$

with their centers on two periodic orbits at the same energy (192.4 K), one on a S type, $(x_{10},x_{20},p_{10},p_{20}) = (0.0,14.9094, 0.0,2.6473)$ and $(\alpha_1,\alpha_2) = (0.37378, 0.37173)$. The second PO is of $I1A$ type with $(x_{10},x_{20},p_{10},p_{20}) = (0.0,14.9094, 3.0572,0.0)$ and the same widths as the S type. The average energy of the wave packets is 209.53 K.

The Fourier transforms of the autocorrelation functions,

$$I(E) = \frac{1}{2\pi\hbar} \int_{-\infty}^{\infty} \exp(iEt/\hbar) \langle \phi(\mathbf{x},0) | \phi(\mathbf{x},t) \rangle dt, \quad (3)$$

are shown in Fig. 5 for the S [Fig. 5(a)] and $I1A$ [Fig. 5(b)] POs, respectively. These markedly different spectra are the result of two excitations with initial Gaussians having the same center in configuration space and widths but differing in their initial phases because of the different momenta of periodic orbits.

Superimposed in Fig. 5(a) we show the calculated spectra using the Fourier pseudospectral method and a variable order FD method ($M = 5$, where the order M is defined from the $N = 2M + 1$ number of grid points used in the centered equi-spaced grid approximation of the second derivatives). The two spectra are practically indistinguishable. We used the same grid spacing and ranges in configuration space for both methods but we generated an optimized grid set in the FD scheme, by selecting those grid points with potential energy below a cutoff value, $V_c = 400$ K. This amounts into reducing the number of grid points from 32 768 in the Fourier PS case (rectangular grid) to 13 338 points, which together with the use of the local approximation allows a reduction in time by a factor of 3. The calculations were done

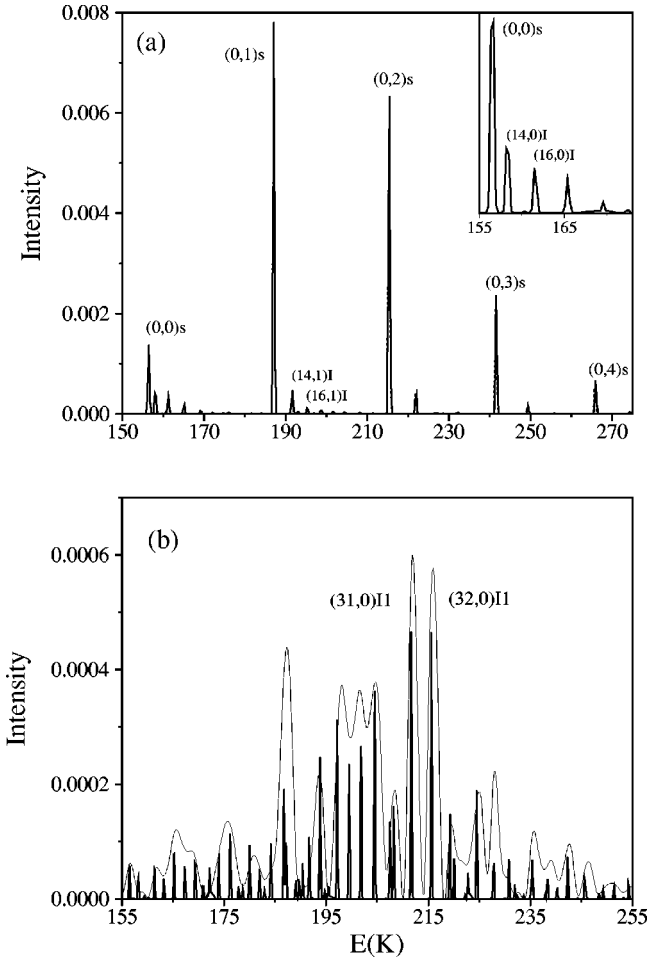

FIG. 5. Power spectra obtained from the quantum mechanical propagation of two Gaussian wave packets with the same widths and centers in configuration space, but differing in phase. In (a) the momentum is given along the x_2 coordinate, and the regular progressions are labeled according to the character of the wave functions (S for excitations along collinear stretching in x_2, I for isomerizing type). With solid lines we plot the spectrum obtained using the FFT method, and with dashed lines the one calculated with a 5th order FD scheme. The differences in the spectra are indistinguishable at the scale of the plot. In panel (b) the momentum is given along the x_1 coordinate. With the thick line we show the spectrum calculated with resolution 0.15 K, and with the thin solid line the spectrum at resolution 1.25 K. Both calculations were carried out with a FD of 5th order.

with and without absorbing boundary conditions and we obtained the same results. This is a consequence of the localization of the wave packet.

We use the spectral method[35] to filter out the eigenfunctions of the most intense peaks in the spectrum of Fig. 5(a). Although spectral methods are not as accurate as filter diagonalization techniques,[36,37] for the present study where we seek a qualitative accuracy, these results are adequate. The progression of the five major lines are assigned to $(0,n)_S$, $n=0-4$ states which are found to be regular and well localized in the region of the transition state as can be seen in Fig. 6. In this figure we plot the square of the eigenfunction and the contours cover the range of 0.1–0.9. The label S is used to denote their association to the S periodic orbits. We note that the ground $(0,0)_S$ state shows some probability amplitude along the reaction path, something which we do not see for the excited states. We attribute this to the chaotic region

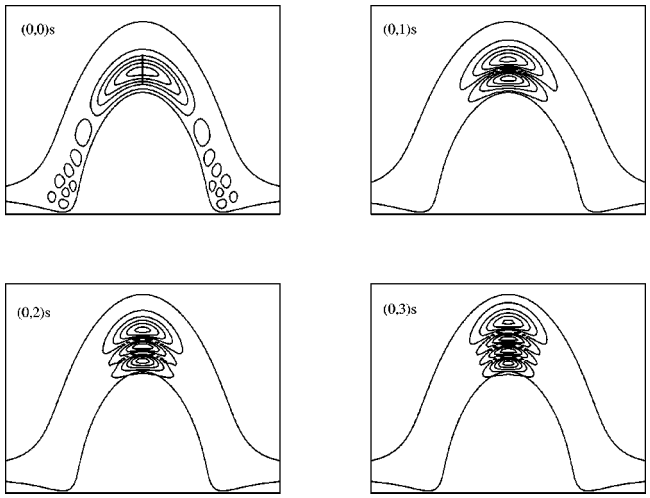

FIG. 6. Regular eigenfunctions of S type obtained from the spectrum of Fig. 5(a). In the upper left panel the periodic orbit of the S family is superimposed.

of phase space with which the wave function overlaps at these energies (156.5 K).

The progressions between two successive major lines in the spectrum of Fig. 5(a) with decreasing intensities are due to wave functions of inversion type. In Fig. 7 we present the $(14,0)_I$ and $(16,1)_I$ states. Superimposed is an $I0$ periodic orbit. Thus, the initial wave packet with a phase along the S periodic orbit excites not only symmetric stretch states but also the inversion states.

Contrary to that, filtering the eigenfunctions which correspond to the most intense peaks of the spectrum in Fig. 5(b) we find only isomerizing type wave functions (Fig. 8).

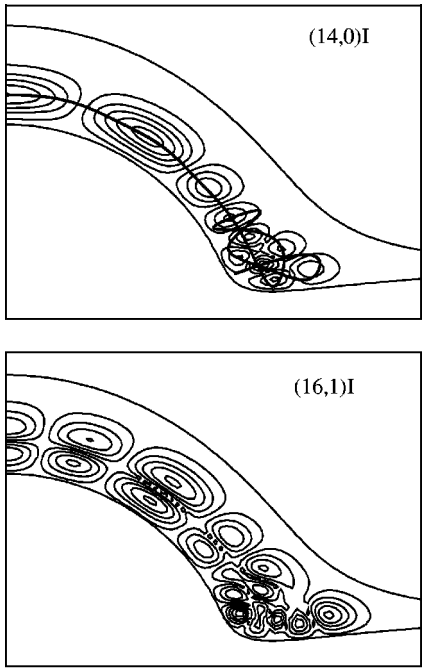

FIG. 7. Wave functions of isomerizing character obtained from the low intensity progressions of the spectrum in Fig. 5(a). They correspond to the eigenstates with energies 158.26 K (up) and 195.92 K (down). Superimposed on the $(14,0)I$ state there is a saddle node PO ($I0$) at the same energy.

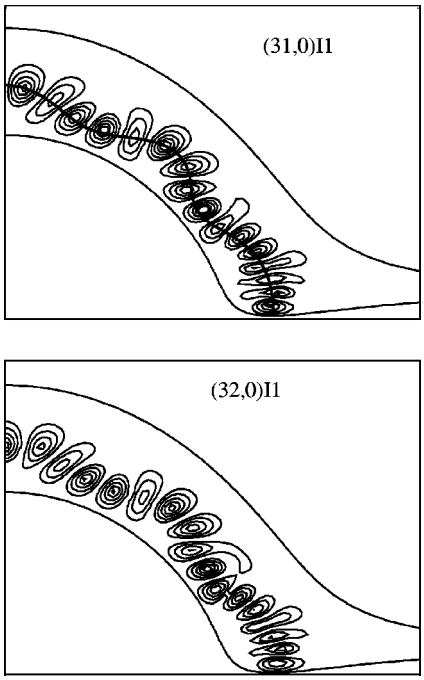

FIG. 8. Filtered eigenfunctions corresponding to the two highest peaks in the spectrum of Fig. 5(b), with energies 211.65 K (up) and 215.58 K (down) showing very good localization on the saddle node PO of the family $I1A$.

The saddle node periodic orbits of the $I2$ family seem to match very well with the $(31,0)_I$ and $(32,0)_I$ eigenstates.

Comparison with the 3D calculations of Wright and Hutson[18] shows that similar eigenfunctions are obtained for states which correspond to the T-shaped Ar_3. Particularly, the localization of states in the region of the transition state (symmetric stretch) as well as the isomerizing regular states are reproduced. Thus, we infer that the inclusion of the third degree of freedom does not alter our conclusions extracted from the T-shaped inversion dynamics.

IV. SUMMARY AND CONCLUSIONS

In the past years several triatomic molecules have been studied within a program which involves the construction of C/B diagrams of the main families of periodic orbits and then the quantum mechanical study of the molecule for the comparison of PO results with the wave functions at particular energies. The periodic orbit method (POM) reveals the dynamical characteristics which are preserved in the quantum world. At high excitation energies localized regular states which correspond to saddle node periodic orbits are now well established.

This program applied to the inversion dynamics of the van der Waals system of Ar_3 surprised us by showing stable periodic orbits at the region of the transition state (collinear geometries). Thus, regular eigenfunctions localized at the same region in configuration space are extracted by filtering a wave packet propagated in time. The most interesting, however, is the production of spectra distinctly different by monitoring the phase of the initial wave packet. It has been shown that wave packets launched onto orthogonal type periodic orbits, S and I, overlap with different type eigenfunctions, the symmetric stretches which inhibit the inversion process and those which promote the inversion process, respectively. This picture remains even when the third degree of freedom is included as recent calculations have shown.[18]

We understand that experimentally it is difficult to study the spectroscopy of Ar_3. However, there is a rich spectroscopy for H_3^+ species for which similar type saddle node periodic orbits have been located. We hope that the present results will stimulate further studies in this system, although we anticipate that the simplicity found in the weakly bound Ar_3, which has a significantly less dense spectrum, can not be achieved.

In the present study we were able to further test a new high order finite difference method for solving the time dependent Schrödinger equation. We demonstrated that although pseudospectral methods based on FFT are fast and quite accurate for 2D systems, FD methods may give equivalent accuracies and even become faster because of the freedom in selecting the grid points. The complex configuration space of Ar_3 makes the FD method more appropriate than the FFT one.

ACKNOWLEDGMENT

R. Guantes gratefully acknowledges financial support from a European Union TMR grant ($FMRX'CT'97'0101$).

[1] S. C. Farantos, Int. Rev. Phys. Chem. **15**, 345 (1996).
[2] See articles in *Molecular Dynamics and Spectroscopy by Stimulated Emission Pumping*, edited by H.-L. Dai and R. Field (World Scientific, Singapore, 1995).
[3] M. C. Gutzwiller, *Chaos in Classical and Quantum Mechanics*, Vol. 1 (Springer-Verlag, Berlin, 1990).
[4] E. J. Heller, Acc. Chem. Res. **14**, 368 (1981).
[5] R. Prosmiti and S. C. Farantos, J. Chem. Phys. **103**, 3299 (1995).
[6] R. Prosmiti, S. C. Farantos, R. Guantes, F. Borondo, and R. M. Benito, J. Chem. Phys. **104**, 2921 (1996).
[7] M. Founargiotakis, S. C. Farantos, H. Skokos, and G. Contopoulos, Chem. Phys. Lett. **277**, 456 (1997).
[8] H. Ishikawa, Y.-T. Chen, Y. Ohshima, B. Rajaram, J. Wang, and R. W. Field, J. Chem. Phys. **15**, 7383 (1996).
[9] H. Ishikawa, C. Nagao, N. Mikami, and R. W. Field, J. Chem. Phys. **109**, 492 (1998).
[10] S. C. Farantos, H.-M. Keller, R. Schinke, K. Yamashita, and K. Morokuma, J. Chem. Phys. **104**, 10 055 (1996).
[11] Ch. Beck, H.-M. Keller, S. Yu. Grebenshchikov, R. Schinke, S. C. Farantos, K. Yamashita, and K. Morokuma, J. Chem. Phys. **107**, 9818 (1997).
[12] H. Ishikawa, R. W. Field, S. C. Farantos, M. Joyeux, J. Koput, C. Beck, and R. Schinke, Annu. Rev. Phys. Chem. **50**, 443 (1999).
[13] J. Tennyson, O. Brass, and E. Pollak, J. Chem. Phys. **92**, 3005 (1990).
[14] S. C. Farantos, Chem. Phys. Lett. **92**, 379 (1982).
[15] T. L. Beck, M. Leitner, and R. S. Berry, J. Chem. Phys. **89**, 1681 (1988).
[16] R. S. Dumont and S. Jain, J. Chem. Phys. **97**, 1227 (1992).
[17] S. Jain, S. Bleher, and R. S. Dumont, J. Chem. Phys. **99**, 7793 (1993).
[18] N. J. Wright and J. M. Hutson, J. Chem. Phys. **110**, 902 (1999).
[19] B. Fornberg, *A Practical Guide to Pseudospectral Methods*, Vol. 1. (Cambridge Monographs on Applied and Computational Mathematics, U.S.A., 1998).
[20] R. Guantes and S. C. Farantos, J. Chem. Phys. **111**, 10827 (1999), preceding paper.
[21] R. A. Aziz and M. J. Slaman, Mol. Phys. **58**, 679 (1986).
[22] S. C. Farantos, Comput. Phys. Commun. **108**, 240 (1998).
[23] E. L. Allgower and K. Georg, *Numerical Continuation Methods*, Vol. 13, A Series in Computational Mathematics (Springer-Verlag, New York, 1990).
[24] R. Seydel, *From Equilibrium to Chaos: Practical Bifurcation and Stability Analysis* (Elsevier, New York, 1988).
[25] E. Reithmeier, *Periodic Solutions of Nonlinear Dynamical Systems*, Lec-

ture Notes in Mathematics (Springer-Verlag, New York, 1991).
[26] R. Kosloff, Annu. Rev. Phys. Chem. **45**, 145 (1994).
[27] B. Fornberg, Math. Comput. **51**, 699 (1988).
[28] R. Kosloff, in *Dynamics of Molecules and Chemical Reactions* , edited by R. E. Wyatt and J. Z. H. Zhang (Marcel Dekker, New York, 1996).
[29] Z. Bacic and J. C. Light, Annu. Rev. Phys. Chem. **40**, 469 (1989).
[30] J. C. Light, I. P. Hamilton, and J. V. Lill, J. Chem. Phys. **82**, 1400 (1985).
[31] D. K. Hoffman, N. Nayar, O. A. Shraraffedin, and D. J. Kouri, J. Phys. Chem. **95**, 8299 (1991).
[32] A. Weinstein, Invent. Math. **20**, 47 (1973).
[33] J. Moser, Pure Appl. Math. **29**, 727 (1976).
[34] M. A. Krasnosel'skii and P. P. Zabreiko, *Geometrical Methods of Nonlinear Analysis*, Vol. 263, A series of comprehensive Mathematics (Springer-Verlag, New York, 1984).
[35] M. D. Feit, J. A. Fleck, and A. Steiger, J. Comput. Phys. **47**, 412 (1982).
[36] V. A. Mandelshtam and H. S. Taylor, J. Chem. Phys. **106**, 5085 (1997).
[37] V. A. Mandelshtam and H. S. Taylor, J. Chem. Phys. **107**, 6756 (1997).